

WAS THE ANDROMEDA STREAM PRODUCED BY A DISK GALAXY?

MARK A. FARDAL^{1,2,3}, ARIF BABUL³, PURAGRA GUHATHAKURTA², KAROLINE M. GILBERT², CARA DODGE^{1,4}

Submitted to Astrophysical Journal Letters

ABSTRACT

The halo region of M31 exhibits a startling level of stellar inhomogeneities, the most prominent of which is the “giant southern stream”. Our previous analysis indicates that this stream, as well as several other observed features, are products of the tidal disruption of a *single* satellite galaxy with stellar mass $\sim 10^9 M_\odot$ less than 1 Gyr ago. Here we show that the specific observed morphology of the stream and halo debris favors a cold, rotating, disk-like progenitor over a dynamically hot, non-rotating one. These observed characteristics include the asymmetric distribution of stars along the stream cross-section and its metal-rich core/metal-poor sheath structure. We find that a disk-like progenitor can also give rise to arc-like features on the minor axis at certain orbital phases that resemble the recently discovered minor-axis “streams”, even reproducing the lower observed metallicity of these streams. Though interpreted by the discoverers as new, independent tidal streams, our analysis suggests that these minor-axis streams may alternatively arise from the progenitor of the giant southern stream. Overall, our study points the way to a more complete reconstruction of the stream progenitor and its merger with M31, based on the emerging picture that most of the major inhomogeneities observed in the M31 halo share a common origin with the giant stream.

Subject headings: galaxies: M31 – galaxies: interactions – galaxies: kinematics and dynamics

1. INTRODUCTION

The relative proximity of the Andromeda galaxy (M31) and the global perspective from our external vantage point make M31 an excellent laboratory for studying the stellar halos of large galaxies. Resolved stellar maps of M31’s halo, assembled over the past decade, have revealed highly complex inhomogeneities, the most striking of which is the Giant Southern Stream (GSS), extending ~ 150 kpc away from M31’s center in the southeast direction (Ibata et al. 2001; Ferguson et al. 2002; McConnachie et al. 2003; Ibata et al. 2007, hereafter I07) and falling towards M31’s center with relative radial velocities as high as ~ 250 km s⁻¹ (Ibata et al. 2004; Guhathakurta et al. 2006; Kalirai et al. 2006). Other significant morphological and kinematic features in the M31 halo include stellar shelves (Ferguson et al. 2002; Fardal et al. 2007; Gilbert et al. 2007, hereafter F07/G07) as well as the recently discovered minor axis “streams” (I07). The GSS is especially notable because it offers an opportunity to precisely measure M31’s potential (Ibata et al. 2004; Fardal et al. 2006, hereafter F06) and provides a view into the most significant Local Group galaxy disruption in the last Gyr.

Models detailing the formation of the GSS agree remarkably well with most aspects of the observations, and suggest the progenitor had a stellar mass of $\sim 2 \times 10^9 M_\odot$ (Font et al. 2006, F06; F07). Our kinematic analysis in F07 finds that seemingly unrelated features like the “Northeast Shelf” and less prominent “West-

ern Shelf” are also the result of the same disruption process (F07), a conclusion supported by independent studies of their stellar populations (Ferguson et al. 2005; Richardson et al. 2008). The observed GSS’s most striking point of contrast with the models is its asymmetry in the transverse direction. As shown both with photometric samples (McConnachie et al. 2003) and spectroscopic surveys (G07), its stellar distribution is sharply truncated on the NE side and falls off much more slowly on the SW side. In addition, the current models do not address the observed stellar population gradients within the GSS (Ferguson et al. 2002; McConnachie 2006, I07).

In this letter, we show that this structure in the GSS can be accounted for if the progenitor hosted a cold, rotating stellar disk, unlike the simple spherical progenitors used in previous simulations. Surprisingly, we find that the disruption of a disk galaxy can also give rise to features similar to the recently discovered arc-like minor-axis “streams”, leading to the tantalizing possibility that most of the major inhomogeneities observed in the M31 halo are tidal debris from the same galaxy that caused the GSS. In Section 2, we briefly describe our model for the progenitor and our *N*-body study of its tidal disruption. In Section 3, we show results from these simulations, focusing on the transverse density profile of the GSS, the metallicity gradient, and arc-like structures that overlap the minor axis. Section 4 summarizes our conclusions.

2. SIMULATION METHOD

Our simulations are based on the methods worked out in our earlier papers: Geehan et al. (2006), F06, and F07. We use the orbit and potential from Table 1 of F07 and their spherical Plummer model to represent a non-rotating progenitor. For runs with a disk progenitor, we use the same initial position and velocity, but substitute a different initial structure of the satellite.

Briefly, our disk models assume the satellite is com-

Electronic address: fardal@astro.umass.edu

¹ Dept. of Astronomy, University of Massachusetts, Amherst, MA 01003, USA

² UCO/Lick Observatory, Dept. of Astronomy & Astrophysics, Univ. of California, 1156 High St., Santa Cruz, CA 95064, USA

³ Dept. of Physics & Astronomy, University of Victoria, Elliott Building, 3800 Finnerty Rd., Victoria, BC, V8P 1A1, Canada

⁴ Astronomy Department, Smith College, Clark Science Center, Northampton, MA 01060, USA

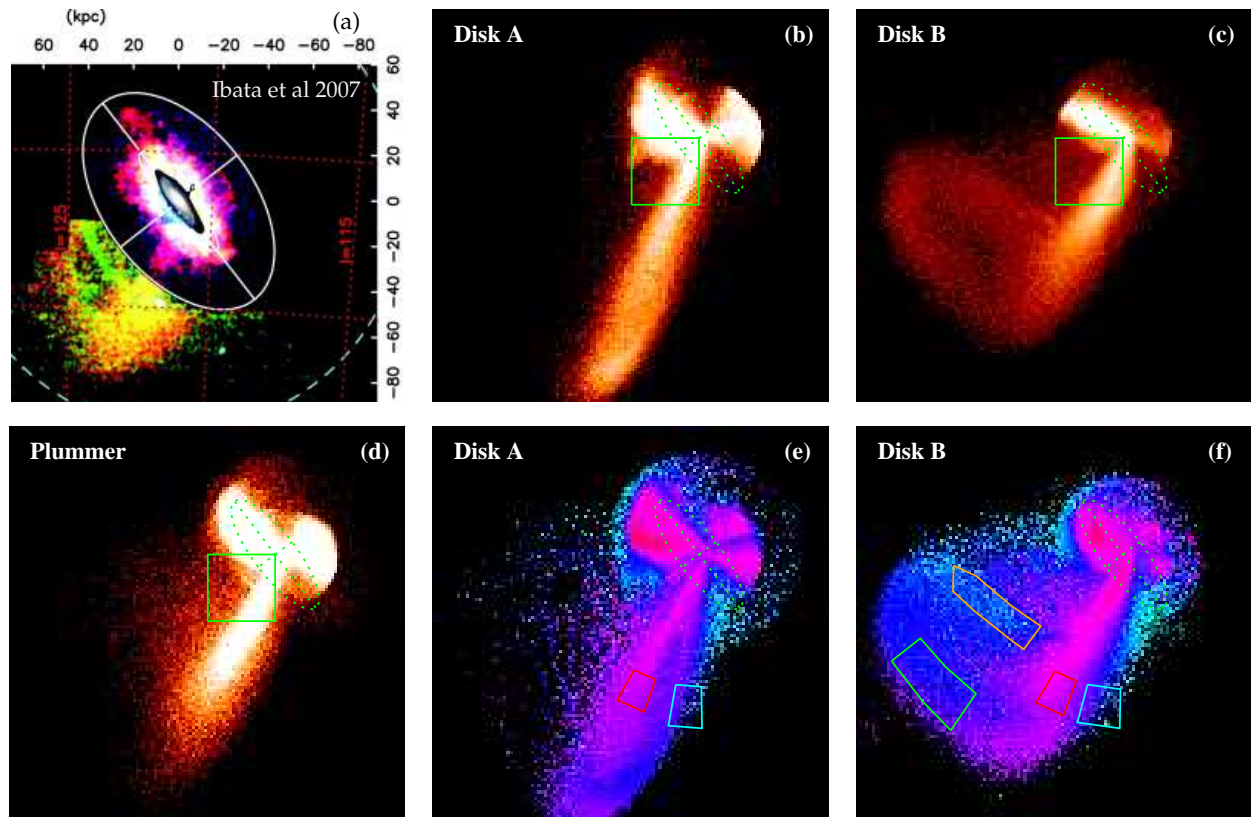


FIG. 1.— (a): Stellar surface density/metallicity map of M31 from I07. The shallower INT/WFC survey is used inside the large ellipse, and the deeper CFHT/MegaCam survey outside it. The minor-axis “streams” C and D are visible at the lower left, projecting from the larger plume of the GSS. These streams (green) and the GSS cocoon (red) are observed to be more metal poor than the GSS core (yellow). (b): Mass surface density map from model Disk A, 840 Myr into the run. The map is 160 kpc on a side, and a dotted contour indicates M31’s disk orientation. The square indicates the region shown in Figure 2. (c): Same for model Disk B, at 680 Myr. (d): Same for the Plummer model, at 840 Myr. (e): Map of the metallicity as a function of position in Disk A (at 840 Myr), with red denoting the highest metallicity, dark blue intermediate, and light blue the lowest (see Figure 3a for a quantitative scale). Boxes indicate the regions used for the metallicity histograms in Figure 3. (f): Same for Disk B (at 680 Myr).

posed of a bulge and rotating disk of stars. For simplicity we assume that the dark matter associated with the galaxy has been tidally stripped before the encounter modeled here. We use a hot exponential sech^2 disk with mass $1.8 \times 10^9 M_\odot$, radial scale length 0.8 kpc, and vertical scale height 0.4 kpc. We add to this a Hernquist bulge of mass $4 \times 10^8 M_\odot$ and scale length 0.4 kpc. We initialize both components with the package ZENO written by Josh Barnes. We evolve the satellite in M31’s potential starting from 12 evenly spaced orientations of the disk. From this we select two models displaying particularly good agreement with observational features, referred to here as Disks A and B. In a forthcoming paper we will conduct a more systematic survey of possible initial conditions and quantify the debris structure in detail (Fardal et al., in preparation).

The remaining details of the simulations are the same as those in F06 and F07. We set the satellite in motion inbound and slightly past apocenter, minimizing initial transients from M31’s tidal forces. We run the simulations with the multisteping tree code PKDGRAV (Stadel 2001). Our simulations include the self-gravity of the progenitor satellite, but ignore dynamical friction, perturbations from the other M31 satellites, and the history of the progenitor prior to the orbit that produces

the GSS, as justified in our earlier papers. We stop the simulations 840 Myr into the run, which is approximately 650 Myr past the initial pericenter. This time was chosen in F07 to give a reasonable match to the debris structure around M31, including the radii of the “shells” on the E and W sides.

3. RESULTS

3.1. Stream morphology

Figures 1b,d show surface density maps based on the Disk A and Plummer models, respectively. Both models reproduce the main feature of a stream extending to the SE. They also reproduce the observed line-of-sight distances and velocities along the GSS. However, the transverse distribution of GSS stars is strikingly different between the two models—Disk A displays a much sharper NE edge. The observed star-count maps (Ferguson et al. 2002, I07) are not directly comparable since they contain both non-GSS-related M31 components and non-M31 contaminants and are not explicitly calibrated to stellar surface density, but the morphology of the GSS in these maps appears much closer to our disk model.

Figure 1d shows that the Plummer model results in a large amount of stars spilling over as far as the SE minor axis, located to the NE of the GSS. When G07

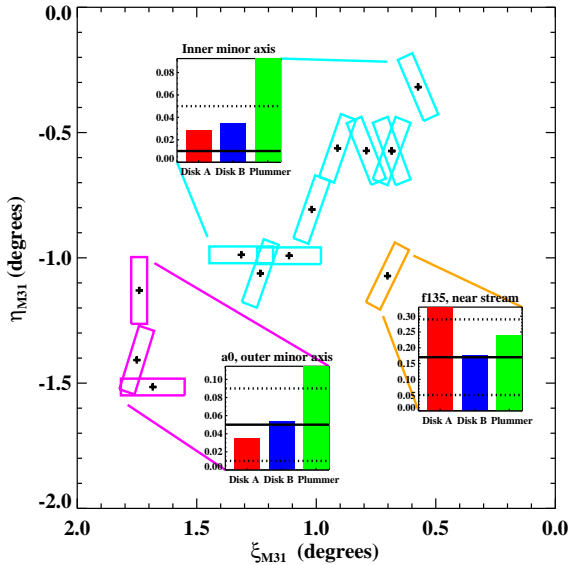


FIG. 2.— Comparison of the minor-axis contamination to the observations of G07. The G07 DEIMOS masks (rectangles) are grouped into inner minor-axis masks, outer minor-axis masks, and a single mask (f135) offset from the minor axis. M31’s center is at (0, 0). The inset plots for each group show the ratio R_m of the strength of the GSS component to the peak of the GSS at the same R_{proj} . R_m is measured as discussed in the text for Disks A and B and the Plummer model 840 Myr into the runs. The observational estimates and $\pm 2\sigma$ error bars from Gilbert et al. (in preparation) are plotted as horizontal solid and dotted lines. The Plummer model clearly contributes too much debris on the minor axis.

compared their Keck/DEIMOS spectroscopic data near M31’s SE minor axis to this model, they noted much less spillover from the GSS than predicted by the model. Gilbert et al. (in preparation) has quantified this by dividing the number of stars moving with GSS-like velocities on the minor axis to those in the GSS core at the same projected radius R_{proj} . For the nine innermost DEIMOS masks on the minor axis combined, this ratio $R_m = 0.01 \pm 0.02$; for the three outermost masks on the minor axis, $R_m = 0.05 \pm 0.02$; and for the mask f135 located somewhat nearer the GSS, they find a likely detection of GSS material with $R_m = 0.17 \pm 0.06$.

In Figure 2, we compare the density of GSS stars in all three N -body models to these results. We have selected “GSS” particles by defining the trend of radial velocity v with R_{proj} and then taking stars that fall within $\pm 80 \text{ km s}^{-1}$ of this velocity in the given field. We also restrict the particles to those actually in the GSS’s “shell”. We then repeat the procedure for a control field located at the peak of the GSS at the same R_{proj} , using a smaller interval $\pm 40 \text{ km s}^{-1}$ as the GSS core has a sharper velocity distribution. Clearly the two disk models are in better accord with the observations than the Plummer model.

The sharper NE edge and smaller minor-axis contamination of the disk models thus imply that the progenitor was rapidly rotating. We will explore this argument in more detail in Fardal et al. (2008, in preparation).

3.2. Metallicity pattern

The mean color of GSS RGB stars is observed to vary in the transverse direction: the GSS is significantly broader in blue than in red stars (Ferguson et al. 2002; McConnachie 2006). This is probably due to a metallic-

ity gradient. I07 quantified the metallicity distribution in two GSS-dominated regions, one in the center of the GSS and one in a less dense “cocoon” region to the SW, and showed that the latter has a lower mean metallicity.

Disk galaxies, of course, tend to have metallicity gradients. Therefore it is interesting to see how a plausible gradient in our disk progenitor translates to the metallicity pattern on the sky.

We use a simple parametric model to produce a plausible metallicity gradient in our initial disk model. We first find the specific orbital energy E_i of each particle. We then assign it a metallicity using $[\text{Fe}/\text{H}] = A_Z + B_Z \log_{10} [-E_i/(50 \text{ km s}^{-1})^2]$, setting A_Z and B_Z to agree with the results of I07 as explained below. This produces the metallicity gradient seen in Figure 3a. Observational results for the stars in the small disk galaxy M33 are also plotted, with the radius for both galaxies normalized by the disk scale length; the metallicity pattern of our disk model agrees quite well. The GSS progenitor should perhaps be lower in metallicity than M33 by a few tenths of dex due to its lower inferred mass, but the photometric metallicity measurements probably have systematic uncertainties at this level in any case.

Figure 1e shows the sky view of the resulting model metallicity pattern. The gradient along the stream is very weak, but the mean metallicity along the denser central part is clearly higher than in the broad wing to the SW, similar to the pattern seen in M31’s GSS. Using I07’s Figure 27, we estimate the “core” and “cocoon” regions (at $R_{\text{proj}} \sim 60 \text{ kpc}$) have mean metallicities of $[\text{Fe}/\text{H}] = -0.54$ and -0.71 , respectively (mean $[\text{Fe}/\text{H}] = -0.51$ was obtained at the GSS’ sharp NE edge by Guhathakurta et al. 2006). Figure 1e shows “broad wing” and “central GSS” boxes chosen at a similar radius, but better matching the slightly different model stream position. Once we set $A_Z = -0.70$ and $B_Z = 1.06$, the metallicities in these boxes are also -0.54 and -0.71 . The bare fact we can match two metallicities with two parameters is not in itself meaningful, but it is significant that the magnitude *and sign* of our initial metal gradient are very reasonable (Fig. 3a). Figure 3b shows that within each box there is a wide range of metallicities; the distributions in I07 appear somewhat broader, but given measurement errors and the contributions from other halo components this is not surprising.

3.3. Minor-axis arcs

Using their MegaCam photometric survey of M31’s halo, I07 found multiple surface density ridges along the minor axis which they called “streams”. Streams C and D (the two closest to M31) form a pair of curving ridges at slightly different orientations, which appear to merge as they approach the survey boundary (see their Fig. 22). Stream C appears to be slightly broader than stream D, and slightly more metal-rich, though not as metal-rich as the GSS core/cocoon. From I07’s Figure 33 we estimate the mean metallicity of streams C and D to be -0.82 and -0.91 respectively. Mori & Rich (2008) suggested these “streams” might be shell features from a satellite disruption, similar to the event that created the GSS but from a different progenitor.

While studying our overall sample of runs based on 12 disk orientations, we noticed one (Disk B) containing two curious “arcs” crossing the minor axis. These

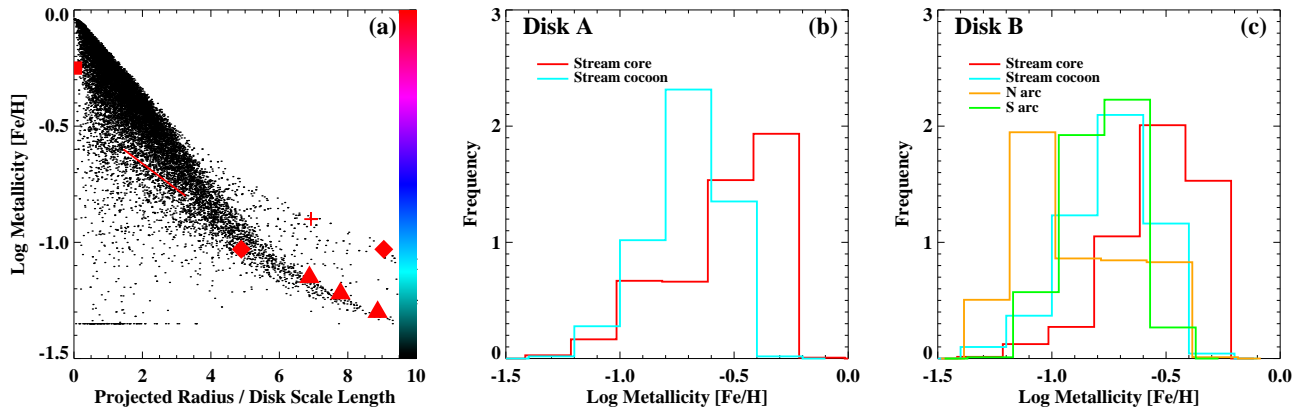


FIG. 3.— (a): Metallicity values in the original disk prior to disruption are shown by black dots, where the radius is plotted in units of disk scale length. For comparison, observed results for M33’s disk stars are plotted as symbols and lines: Stephens & Frogel (2002) (square); linear approximation to points of Kim et al. (2002) (straight line); Galleti et al. (2004) (diamonds); McConnachie et al. (2006) (cross); Barker et al. (2007) (triangles). The colorbar translates $[\text{Fe}/\text{H}]$ to the color scale of Figures 1e,f. (b): Histogram of particle metallicity values in model Disk A within the “core” and “cocoon” regions marked in Figure 1e. (c): Histogram of particle metallicity values in model Disk B within the “core”, “cocoon”, “N arc”, and “S arc” regions marked in Figure 1f.

arcs are clearest at the step 680 Myr into the run shown in Figure 1c. Morphologically, the two arcs somewhat resemble streams C and D, with a fatter southern arc nearly merging into a sharper northern arc. Like the observed “streams”, neither arc crosses the GSS to the SW. Compared to the observed arcs, the simulated arcs are significantly further from M31’s center.

As Figure 1f shows, the simulated arcs are significantly less rich in metals than the GSS. Using the same metallicity model as for Disk A and the regions defined by boxes in this figure, the mean $[\text{Fe}/\text{H}]$ is -0.78 for the southern arc and -0.90 for the northern arc. Thus there is considerable if inconclusive evidence that these arcs are close analogues of the “streams” in I07.

In our model, these two arcs originate from the outer regions of the disk, and are sharp mainly because of the relatively cold velocity field of the disk. Both arcs consist of material that takes a path around M31’s center nearly opposite to the bulk of the progenitor, explaining why they lie so far from the GSS. The large size of our disk is thus crucial; a compact progenitor resembling M32, for example, would be unable to produce similar arcs. The southern arc consists of a group of particles sharing nearly the same energy, and come from fairly far out in the progenitor’s disk. The northern arc consists of particles that lie even further out (explaining its lower metallicity on average), which form a tidal tail during the interaction with M31.

We cannot yet explore the full parameter space of the collision for the presence and properties of these arc-like features. However, we did conduct a few additional runs with changes to the disk mass, radius, and orientation of Disk B, finding the arcs were sensitive to the exact input parameters. Thus we will require more theoretical investigation as well as more observational constraints to determine whether the arcs explain some of the I07 minor-axis streams, or are merely a fortuitous similarity. If the arcs are shown to be related to the GSS, they will be a very solid argument for the disk nature of the progenitor, and will place strong constraints on the parameters of the collision.

4. CONCLUSIONS

In summary, several strands of observational evidence suggest that the GSS originated from a progenitor with a strong sense of rotation, such as a disk galaxy. The transverse density profile of the GSS is more easily produced by a rotating satellite. The observed decline in mean metallicity from the central core of the GSS to its “cocoon” to the SW suggests that the progenitor had a strong radial metallicity gradient, of the sort found mainly in disk galaxies. Furthermore, several observed arcs lying across the minor axis in M31 have very suggestive analogues in one of our runs. If shown to be related to the GSS in the manner suggested by our model, these features would be definite confirmation of a disk-like progenitor.

The notion of a disk galaxy progenitor is somewhat at odds with age measurements of the GSS, which suggests little star formation during the last 4 Gyr (Brown et al. 2006a,b). However, the fields used to infer this were placed in the central, metal-rich part of the GSS; it is possible that the progenitor had an age gradient as well as a metallicity gradient, with the older stars on the inside. Age measurements in the GSS cocoon would therefore be interesting. It is also possible that the GSS progenitor was more similar to an S0 galaxy than a spiral, perhaps due to stripping of its gas in an earlier phase of its encounter with M31.

Many papers have used metallicity to assess the relationship among various M31 disk and halo features. Our suggestion that the GSS progenitor had a strong metallicity gradient means that metallicity can no longer be used as a reliable fingerprint of origin. This obviously complicates the forensic reconstruction of M31’s merger history. Despite this, the rapidly growing database on M31 halo structure is a fascinating puzzle, offering unique insight into the life of a typical disk galaxy and the death of its unfortunate former companions.

We thank Tom Quinn and Joachim Stadel for the use of PKDGRAV, Josh Barnes for the use of ZENO, and Alan McConnachie and Roger Davies for helpful conver-

sations.

REFERENCES

- Barker, M. K., Sarajedini, A., Geisler, D., Harding, P., & Schommer, R. 2007, *AJ*, 133, 1125
- Brown, T. M., Smith, E., Guhathakurta, P., Rich, R. M., Ferguson, H. C., Renzini, A., Sweigart, A. V., & Kimble, R. A. 2006a, *ApJ*, 636, L89
- Brown, T. M., Smith, E., Ferguson, H. C., Rich, R. M., Guhathakurta, P., Renzini, A., Sweigart, A. V., & Kimble, R. A. 2006b, *ApJ*, 652, 323
- Fardal, M. A., Babul, A., Geehan, J. J., & Guhathakurta, P. 2006, *MNRAS*, 366, 1012 (F06)
- Fardal, M. A., Guhathakurta, P., Babul, A., & McConnachie, A. W. 2007, *MNRAS*, 380, 15 (F07)
- Ferguson, A. M. N., Irwin, M. J., Ibata, R. A., Lewis, G. F., & Tanvir, N. R. 2002, *AJ*, 124, 1452
- Ferguson, A. M. N., Johnson, R. A., Faria, D. C., Irwin, M. J., Ibata, R. A., Johnston, K. V., Lewis, G. F., & Tanvir, N. R. 2005, *ApJ*, 622, L109
- Font, A., Johnston, K. V., Guhathakurta, P., Majewski, S. R., & Rich, R. M. 2006, *AJ*, 131, 1436
- Galletti, S., Bellazzini, M., & Ferraro, F. R. 2004, *A&A*, 423, 925
- Geehan, J. J., Fardal, M. A., Babul, A., Guhathakurta, P. 2006, *MNRAS*, 366, 996
- Gilbert, K. M., et al. 2007, *ApJ*, 668, 245 (G07)
- Guhathakurta, P., et al. 2005, arXiv preprint (astro-ph/0502366)
- Guhathakurta, P., et al. 2006, *AJ*, 131, 2497
- Ibata, R., Irwin, M. J., Ferguson, A. M. N., Lewis, G., & Tanvir, N. 2001, *Nature*, 412, 49
- Ibata, R., Chapman, S., Ferguson, A. M. N., Irwin, M., Lewis, G., & McConnachie, A. 2004, *MNRAS*, 351, 117
- Ibata, R., Martin, N. F., Irwin, M., Chapman, S., Ferguson, A. M. N., Lewis, G. F., & McConnachie, A. W. 2007, *ApJ*, 671, 1591 (I07)
- Kalirai, J. S., Guhathakurta, P., Gilbert, K. M., Reitzel, D. B., Majewski, S. R., Rich, R. M., & Cooper, M. C. 2006, *ApJ*, 641, 268
- Kim, M., Kim, E., Lee, M. G., Sarajedini, A., & Geisler, D. 2002, *AJ*, 123, 244
- McConnachie, A. W., Irwin, M. J., Ibata, R. A., Ferguson, A. M. N., Lewis, G. F., & Tanvir, N. 2003, *MNRAS*, 343, 1335
- McConnachie, A. 2006, *The Observatory*, 126, 144, available at <http://www.astro.uvic.ca/~alan/thesis.pdf>
- McConnachie, A. W., Chapman, S. C., Ibata, R. A., Ferguson, A. M. N., Irwin, M. J., Lewis, G. F., Tanvir, N. R., & Martin, N. 2006, *ApJ*, 647, L25
- Mori, M., & Rich, R. M. 2008, *ApJ*, 674, L77
- Richardson, J. C., et al. 2008, ArXiv e-prints, 803, arXiv:0803.2614
- Stadel, J. 2001, Ph.D. thesis, University of Washington
- Stephens, A. W., & Frogel, J. A. 2002, *AJ*, 124, 2023